



HAL
open science

Hybrid Amyloid-Based Redox Hydrogel for Bioelectrocatalytic H₂ Oxidation

Nicolas Duraffourg, Maxime Leprince, Serge Crouzy, Olivier Hamelin, Yves Usson, Luca Signor, Christine Cavazza, Vincent Forge, Luca Albertin

► **To cite this version:**

Nicolas Duraffourg, Maxime Leprince, Serge Crouzy, Olivier Hamelin, Yves Usson, et al.. Hybrid Amyloid-Based Redox Hydrogel for Bioelectrocatalytic H₂ Oxidation. *Angewandte Chemie International Edition*, 2021, 60 (26), pp.14488-14497. 10.1002/anie.202101700 . hal-03241503

HAL Id: hal-03241503

<https://hal.science/hal-03241503v1>

Submitted on 28 May 2021

HAL is a multi-disciplinary open access archive for the deposit and dissemination of scientific research documents, whether they are published or not. The documents may come from teaching and research institutions in France or abroad, or from public or private research centers.

L'archive ouverte pluridisciplinaire **HAL**, est destinée au dépôt et à la diffusion de documents scientifiques de niveau recherche, publiés ou non, émanant des établissements d'enseignement et de recherche français ou étrangers, des laboratoires publics ou privés.

Hybrid amyloid-based redox hydrogel for bioelectrocatalytic H₂ oxidation

Nicolas Duraffourg,^[a] Maxime Leprince,^[a] Serge Crouzy,^[a] Olivier Hamelin,^[a] Yves Usson,^[b] Luca Signor,^[c] Christine Cavazza,^[a] Vincent Forge^[a] and Luca Albertin*^[a]

Dedicated to the memory of Dr. Serge Crouzy

- [a] Dr N. Duraffourg, M. Leprince, Dr. S. Crouzy, Dr O. Hamelin, Dr C. Cavazza, Dr V. Forge, and Dr L. Albertin
Univ. Grenoble Alpes, CNRS, CEA, IRIG, Laboratoire de Chimie et Biologie des Métaux, 38000 Grenoble, France
E-mail: luca.albertin@cea.fr
- [b] Dr. Y. Usson
Univ. Grenoble Alpes, CNRS, CHU Grenoble Alpes, Grenoble INP*, TIMC-IMAG, 38000 Grenoble, France
- [c] Dr. L. Signor
Univ. Grenoble Alpes, CEA, CNRS, IRIG, IBS, 38000 Grenoble, France

Supporting information for this article is given via a link at the end of the document.

Abstract: An artificial amyloid-based redox hydrogel was designed for mediating electron transfer between a [NiFeSe] hydrogenase and an electrode. Starting from a mutated prion-forming domain of fungal protein HET-s, a hybrid redox protein containing a single benzyl methyl viologen moiety was synthesized. This protein was able to self-assemble into structurally homogenous nanofibrils. Molecular modelling confirmed that the redox groups are aligned along the fibril's axis, and are tethered to its core via a long, flexible polypeptide chain that allows close encounters between the fibril-bound oxidized or reduced redox groups. Redox hydrogel films capable of immobilizing the hydrogenase under mild conditions at the surface of carbon electrodes, were obtained by a simple pH jump. In this way, novel bioelectrodes for the electrocatalytic oxidation of H₂ were fabricated that afforded catalytic current densities of up to 270 $\mu\text{A cm}^{-2}$, with an overpotential of 0.33 V, under quiescent conditions at 45°C.

Introduction

Efficient electrocatalysts are needed in technological applications ranging from energy conversion and storage, to biofuel cells, and the production of electrofuels, commodity chemicals and materials.^[1] In nature, all biological systems extract energy and nutrients from their environment and carry out the metabolic processes associated with life with high molecular and energetic efficiency. Redox enzymes - a particular class of biocatalysts - catalyse many of the reactions involved in these processes, and the design, fabrication, and use of enzyme-modified electrodes is an active field of research.^[2]

Potential advantages of enzymatic bioelectrocatalysis over non-biological systems are as follows: i) higher energy efficiency, due to lower applied overpotentials; ii) very high catalytic activities

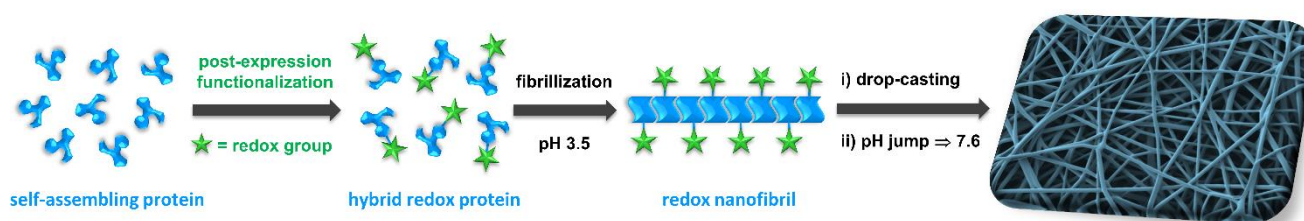
(TOF); iii) excellent product selectivity, decreasing the need for downstream purification; and iv) greatly decreased reliance on non-aqueous solvents and precious metals.

A major challenge in bioelectrocatalysis is to establish electrical communication between enzymes and electrode surfaces:^[1a] most enzymes have an active centre buried deep beneath their surface and surrounded by an insulating protein shell, which prevents direct electron transfer (DET) with the electrode.^[3] Although DET is easier for enzymes with built-in electron transfer pathways, such as hydrogenases,^[4] the enzyme still needs to be adsorbed on the surface of the electrode with an appropriate orientation, so that the most accessible electron relay is close enough to the electrode to allow tunnelling.^[5]

Redox hydrogels - i.e. cross-linked polymer networks featuring reversible redox moieties tethered to their backbone chains - are the only electron-conducting phase in which water-soluble chemicals and biochemicals can dissolve and diffuse.^[6] Accordingly, they are of much interest in bioelectrocatalysis, since they can immobilize a wide range of embedded enzyme molecules, irrespective of their spatial orientation and distance, while allowing the diffusion of reactants, products and ions to and from the bulk of the solution. Moreover, self-standing redox hydrogel films immobilize the biocatalyst within a hydrophilic and solvated matrix that protects it from denaturation.^[7]

Amyloid-based hydrogels (AbHs)^[8] are water-swollen, three-dimensional networks formed by cross-linking of protein fibrils with a structure rich in cross- β -sheets.^[9] The exact mechanism of gelation is complex and varies from one system to another, but involves a combination of non-covalent interactions (i.e. hydrogen bonding, hydrophobic and electrostatic interactions) and entanglement of the fibrils.^[8, 9c, 10] The ability of AbHs to hold large amounts of water is due to the large number of hydrophilic and charged functional groups present on the surface of protein fibrils.

* Institute of Engineering Univ. Grenoble Alpes



Scheme 1. Synthesis of redox nanofibrils from a self-assembling hybrid protein and preparation of amyloid-based redox hydrogel films.

Together with viscoelasticity, these physical properties make AbHs good mimics of the cytosol, extracellular matrix, and biofilms in which many enzymes and bacteria have evolved and/or normally function. Hence, the development of electron-conducting AbHs would enable their use as biomimetic, immobilizing matrices for bioelectrocatalysis.

Baldwin et al.^[11] first proposed the use of amyloid fibril scaffolds to display redox proteins in a linear array in order to favour inter-protein electron transfer via conformational sampling at the protein–protein interface and, ultimately, electron transfer over long distances.^[12] Rengaraj et al.^[13] and Altamura et al.^[14] then applied this concept to the preparation of protein nanowires featuring a contiguous alignment of metalloproteins on their surface. To this end, they exploited the ability of the prion-forming domain (PFD; residues 218 to 289) of the heterokaryon incompatibility protein HET-s from the fungus *P. anserina* (HET_{PFD})^[15] to self-organize into amyloid fibrils with high structural homogeneity, and to do so in a reproducible way even when fused to another protein domain of comparable size.^[16] Therefore, they constructed a fusion protein comprising a small rubredoxin from *Methanococcus voltae* connected to the C-terminus of HET_{PFD}. Following a pH jump, these nanowires self-assembled into redox hydrogel films capable to mediate electron-transfer between an electrode and an imbedded laccase^[14] or [NiFe] hydrogenase.^[13] This work demonstrated the possibility of developing amyloid-based redox hydrogels (AbRxHs) and using them in bioelectrocatalysis. In theory, by changing the nature of the metalloprotein displayed on the fibrils' surface, one could design AbRxH spanning the whole potential window of redox proteins, i.e. -700 to +700 mV vs SHE,^[17] thus allowing their application in a wide range of electrochemical and photoelectrochemical devices.^[7] In practice, however, the need to purify the PFD-containing fusion protein under denaturing conditions limits its scope to redox domains that are either extremely stable or that can be easily refolded in their holo form once the chaotropic agent removed. Furthermore, (i) the active centre of the redox domain has to be close enough to the surface as to allow effective interprotein electron transfer; (ii) its longitudinal size along the fibril axis should not lead to steric hindrance and prevent self-association of the fusion protein; and (iii) a new fusion protein has to be designed, expressed, and refolded whenever the potential of the redox matrix has to be changed.

A more versatile approach the design of AbRxHs (Scheme 1) would involve: (i) production of a self-associating protein carrying one or more functional group(s) amenable to orthogonal chemical functionalization; (ii) site-selective conjugation of artificial prosthetic group(s) (e.g. metal complex or organic molecule) possessing redox or catalytic properties matching the target application; (iii) self-association of the resulting hybrid construct

into redox nanofibrils and gels. Thus, a single protein could serve as platform for the design of AbRxH possessing varying electrochemical and catalytic properties. Interestingly, nanofibrils of HET_{PFD} are highly stable in aqueous solution thanks to the numerous intra- and inter-molecular hydrogen bonds and salt-bridges between β -strands. The structure of the fibrils is known at atomic resolution,^[18] and is not influenced by the mutation of a few amino acids outside the hydrophobic core of the solenoid or the C-terminal semiflexible loop.^[19] Also, their morphology can be controlled by tuning the electrostatic interaction of individual fibrils via pH and ionic strength of the solution.^{[20] [21]}

We therefore postulate that HET_{PFD} could serve as self-associating building block for the rational design of AbRxHs in which the position of artificial prosthetic group(s) along the fibril can be finely controlled by choosing the appropriate anchoring point in the polypeptide chain. In this manner, gel matrices could be engineered for mediated electron transfer (MET) from an electrode to an enzyme or for more complex electrocatalytic reactions involving multiple redox and catalytic sites. Here, we report the first use of such a strategy, in which the [NiFeSe]-hydrogenase from *Desulfomicrobium baculatum* (DbH-[NiFeSe])^[22] was wired to carbon electrodes via a self-assembled AbRxH prepared from a hybrid prion forming domain. DbH-[NiFeSe] was selected because it has one of the highest catalytic activities toward H₂ oxidation among the NiFe hydrogenases (TOF = 4000 s⁻¹),^[22] and because – like other [NiFeSe]-hydrogenases – it is inactivated under oxidizing electrochemical conditions. The latter aspect allows a comparison with previously reported Nernst buffers for this class of enzymes.^[5, 23]

Results and Discussion

Synthesis and structure of redox nanofibrils

A mutant of HET_{PFD} possessing a single cysteine residue at the N-terminus and a His6 tag at the C-terminus (CysHET_{PFD}) was constructed as self-associating building block that can be selectively functionalized via sulfhydryl chemistry.^[24] The protein does not contain Met residues and, at pH values near neutrality, Cys is alkylated by water-soluble benzyl bromide derivatives considerably faster than any other amino acid.^[25]

Recombinant CysHET_{PFD} ($M_r = 9037.0$ g mol⁻¹, theoretical pI = 7.24) was produced by heterologous overexpression in *E. Coli* and 80–140 mg of purified protein were obtained per litre of shake culture (i.e. 40–70 mg of per gram of wet cells; see Figure S1 and S2). Unfolded (monomeric) CysHET_{PFD} was conjugated to bromobenzyl methyl viologen (40 eq.) by nucleophilic substitution under denaturing conditions (GuHCl 5M, pH 7.3, 20°C; Scheme

RESEARCH ARTICLE

S2). Benzyl methyl viologen (BMV) was chosen as redox relay since viologen moieties undergo efficient electron transfer with hydrogenases either in freely diffusing^[26] or polymer-bound forms.^[27] Also, they display fast reaction kinetics with O_2 ,^[28] thus enabling the design of redox hydrogels that protect (bio)catalysts against oxygen damage (although protection from O_2 was not explored in this study).^[23, 27d, 29]

After purification by affinity chromatography, MALDI-TOF-MS analysis confirmed that the isolated protein (BMV-HET_{PFD}) featured a single benzyl methyl viologen group (Figure S3), whose absorbance band at 260 nm is clearly visible in the UV-Vis absorbance spectrum (Figure S4a). When a deoxygenated solution of hybrid protein was reduced with sodium dithionite under Ar, the solution turned blue-violet in color and the characteristic absorbance bands of a monomeric (398, 604 and 732 nm) and dimeric (370, 560 and 880 nm) bipyridinium radical cation appeared in its absorption spectrum (Figure S4b).^[30]

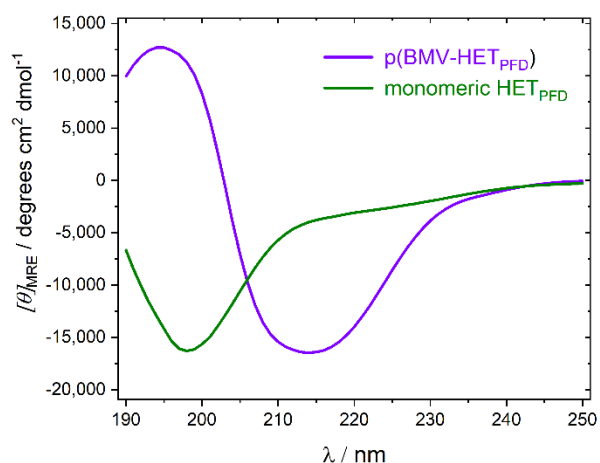


Figure 1. CD spectrum of p(BMV-HET_{PFD}) redox nanofibrils (0.1 mM HCl pH ~3.5) and of the unfolded prion-forming domain (AcOH 1% v/v pH 2.6) in the UV region. Upon polymerization, a transition occurs from a disordered conformation to one rich in β -strands, with a pronounced minimum at 214 nm.^[31]

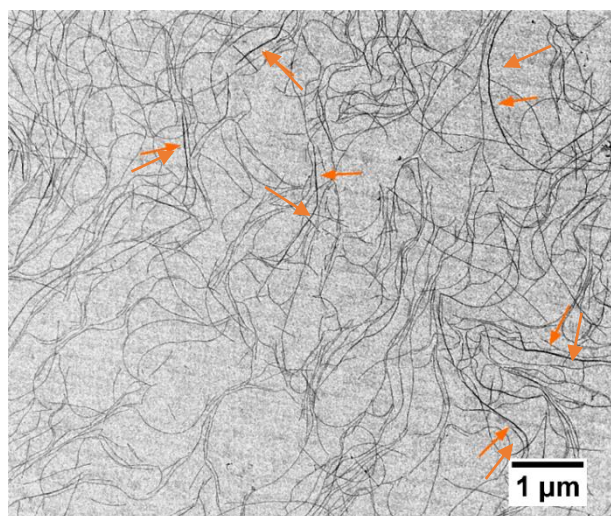


Figure 2. Low voltage TEM image of p(BMV-HET_{PFD}) in 0.1 mM HCl pH 3.5: the sample mostly consists of single-stranded fibrils with some double- and triple-stranded fibres, a few examples of which are indicated by arrows.

Self-association of the hybrid protein (0.13 mM in AcOH 1%) was induced by consecutive buffer exchange (citrate 20 mM pH 3.6, then HCl ~0.1 mM), and progress of fibrillation was monitored by circular dichroism through the appearance of a positive peak at 195 nm and a negative peak at 214 nm (Figure 1), both characteristic of the β -strand conformation predominant in amyloid structures.^[31]

Fibrillation was complete after 23 hours and the length and morphology of the fibrils was observed by low voltage TEM without staining (Figure 2, Figure S6). Single-stranded fibrils of BMV-HET_{PFD} - hereafter indicated as p(BMV-HET_{PFD}) - were predominant but coexisted with double- and triple-stranded fibres resulting from lateral association. Analogous findings were reported for fibrils of wild type HET_{PFD} prepared under similar conditions,^[32] confirming the limited impact of the small artificial prosthetic group on fibrils' morphology.

Measurement of a small sample of individual fibrils ($n=100$) in TEM images indicates that number average contour length was $L_n \cong 1.4 \mu\text{m}$ (which corresponds to an average length / width aspect ratio of 350) and that fibrils were heterogeneous in length ($0.2 \mu\text{m} \leq L \leq 3.7 \mu\text{m}$, $\sigma = 0.9 \mu\text{m}$). The L_n value obtained in this manner is certainly underestimated, since long individual fibrils are more difficult to identify due to their tendency to intertwine and overlap with other fibrils; and because they often extend beyond the visualization area of a TEM image.

Starting from a 5-repeat structure of fibrils of HET-s(218-289) resolved by ssNMR (PDB 2RNM),^[18b] a 12-repeat model for p(BMV-HET_{PFD}) fibrils was built by Molecular Dynamics simulation and energy minimization. As shown in Figure 3, benzyl-methyl-viologen groups are loosely aligned along the fibril axis and anchored at 9.4 Å intervals to the central β -solenoid via a flexible polypeptide chain 10 amino acids long. By exploring its conformational space in solution, the latter enables close encounters between redox relays of proteins that are up to four positions apart along the fibril axis, i.e. overcoming up to four consecutive functionalization defects in the fibril. This encounters support self-exchange reactions among the nanofibril-bound oxidized/reduced redox groups and, ultimately, MET between the hydrogenase and the electrode.

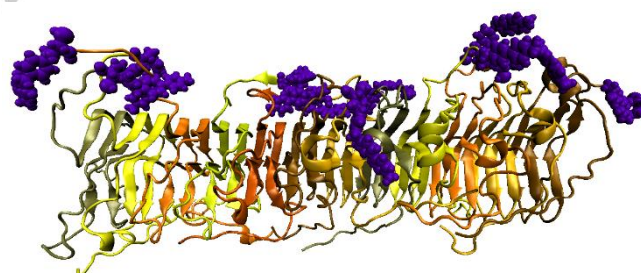


Figure 3. Model of p(BMV-HET_{PFD}) fibril. Different colours indicate different polypeptide chains; benzyl methyl viologen groups are shown in purple.

Amyloid-based redox hydrogels - AbRxHs

Nanofibrils of p(BMV-HET_{PFD}) expose a majority of acidic, basic, hydrophilic and positively charged residues on their surface (Figure S7), among which hydrophobic patches are interspersed.

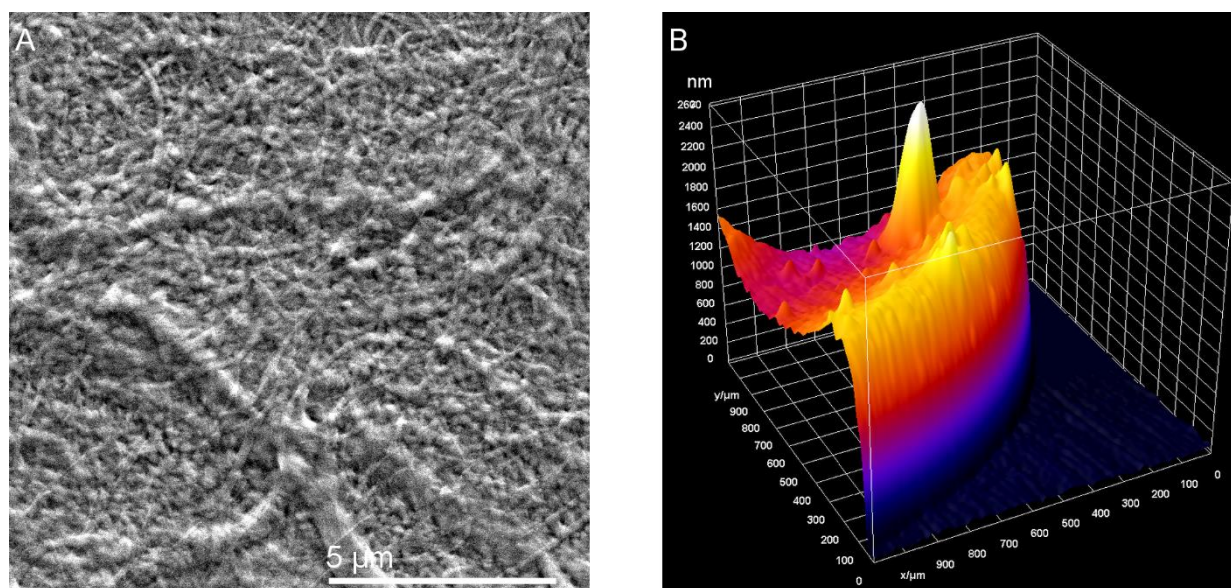


Figure 4. (a) SEM image of a dried single-layer p(BMV-HET_{PFD}) gel film formed on a glassy carbon electrode. b) Topography of an analogous film drop-cast on a borosilicate glass slide (drop volume 2.5 μL) as recorded by DHM. Films of circular shape ~ 2 mm in diameter were typically obtained, and only quarter discs could be imaged by DHM. The scale of the z-axis is nm, whereas x and y axis are in μm .

At $\text{pH} < 4$ and low ionic strength, lateral association is unfavourable due to electrostatic repulsion between positively charged fibrils and, at low concentration, a majority of single-stranded filaments are observed under these conditions (Figure 2, Figure S6). At higher pH values though, net surface charge will be much diminished and electrostatic attraction between oppositely charged patches, as well as hydrophobic interaction between nonpolar patches, will lead to later association of nanofibrils into larger fibres and bundles.

We hypothesised that, above a critical fibril overlap concentration, a sudden decrease in net surface charge would result in a 3D supramolecular network of entangled nanofibres of varying morphology, cross-linked by physical junction zones. Accordingly, the initial suspension of positively charged nanofibrils in 0.1 mM HCl was concentrated 5 $\frac{1}{2}$ fold by ultrafiltration ($c_{\text{final}} \cong 3.8 \text{ g L}^{-1}$), and films were prepared by drop casting 2.0 μL to 4.0 μL onto planar surfaces, followed by drying of the sessile droplet in the open atmosphere. Simple rehydration in the supporting electrolyte used for electrochemical experiments (TrisHCl 20–50 mM / NaCl 50 mM, pH 7.6) effected both later association of the fibrils into larger fibres and their physical cross-linking, yielding transparent hydrogel films.

Figure 4 a shows a SEM image of the dried gel coating a glassy carbon electrode: as expected, it is a dense and intricate network of fibres and bundles with lateral dimension of 100–150 nm and 400–700 nm, respectively (see Figure S8a for more SEM images). The profile of the dried film before physical cross-linking was recorded by stylus profilometry and indicates a thickness varying from 1.7 μm to 3.0 μm with some accumulation of material both at the centre and at the outer rim of the circular deposit (drop volume 3.0 μL , film diameter 2.5 mm; Figure S9). Departure from a flat film morphology is often observed in films obtained by drop-casting methods and it is the result of a complex interplay between mass and heat transport processes taking place within the drying droplet.^[33] In our case though, film inhomogeneity is much less pronounced than the “coffee-ring effect” reported for

branched and dendritic viologen-polyethylenimine solutions drop-cast under similar non-gelling conditions.^[34]

To gain a better insight into the morphology of swollen electroactive and electrocatalytic films, the topography of various AbRxHs was investigated by Digital Holographic Microscopy (DHM) in transmission mode.^[35] DHM is a quantitative phase microscopy technique that enables full-field imaging of the structure and dynamics of transparent samples from a single recorded hologram. Vertical accuracy as low as a few tens of nanometers is achievable under adequate conditions.^[35b]

Circular films 2 mm \pm 0.1 mm in diameter were obtained by drop-casting 2.0 μL of nanofibrils’s suspension onto borosilicate glass slides (as measured by optical microscopy). Quarter films were imaged by DHM both in the dry and hydrogel state (Figure S11). Although surface energy and roughness of the glass slides used for DHM differ from that of GC, the radial profile obtained for a dry single-layer p(BMV-HET) film (Figure 4 b and Figure S9) is similar to that observed by stylus profilometry with a peak-to-valley ratio of ~ 1.7 . The fact that absolute thickness is smaller in the DHM experiment compared to stylus profilometry is probably the result of the smaller volume applied (2.0 μL vs 3.0 μL). Rehydration and cross-linking in the supporting electrolyte swelled the film without any variation in diameter, while the overall profile was maintained. This property is important for ensuring reproducibility of the coating process.

Electrochemistry and bioelectrocatalysis with AbRxHs

Cyclic voltammograms of p(BMV-HET_{PFD}) hydrogel films on Glassy Carbon (GC) and Edge Plane Pyrolytic Graphite (EPPG) electrodes (Figure 5 a, b) display a reversible redox couple with half wave potential $E_{1/2}$ of -0.29 V and -0.28 V, respectively, at all tested scan rates; i.e. a value 0.12 V higher than the formal potential of the $\text{Vio}^{++}/\text{Vio}^{+}$ redox couple of free BMV in solution ($E_{1/2} = -0.408 \text{ V}$).^[36]

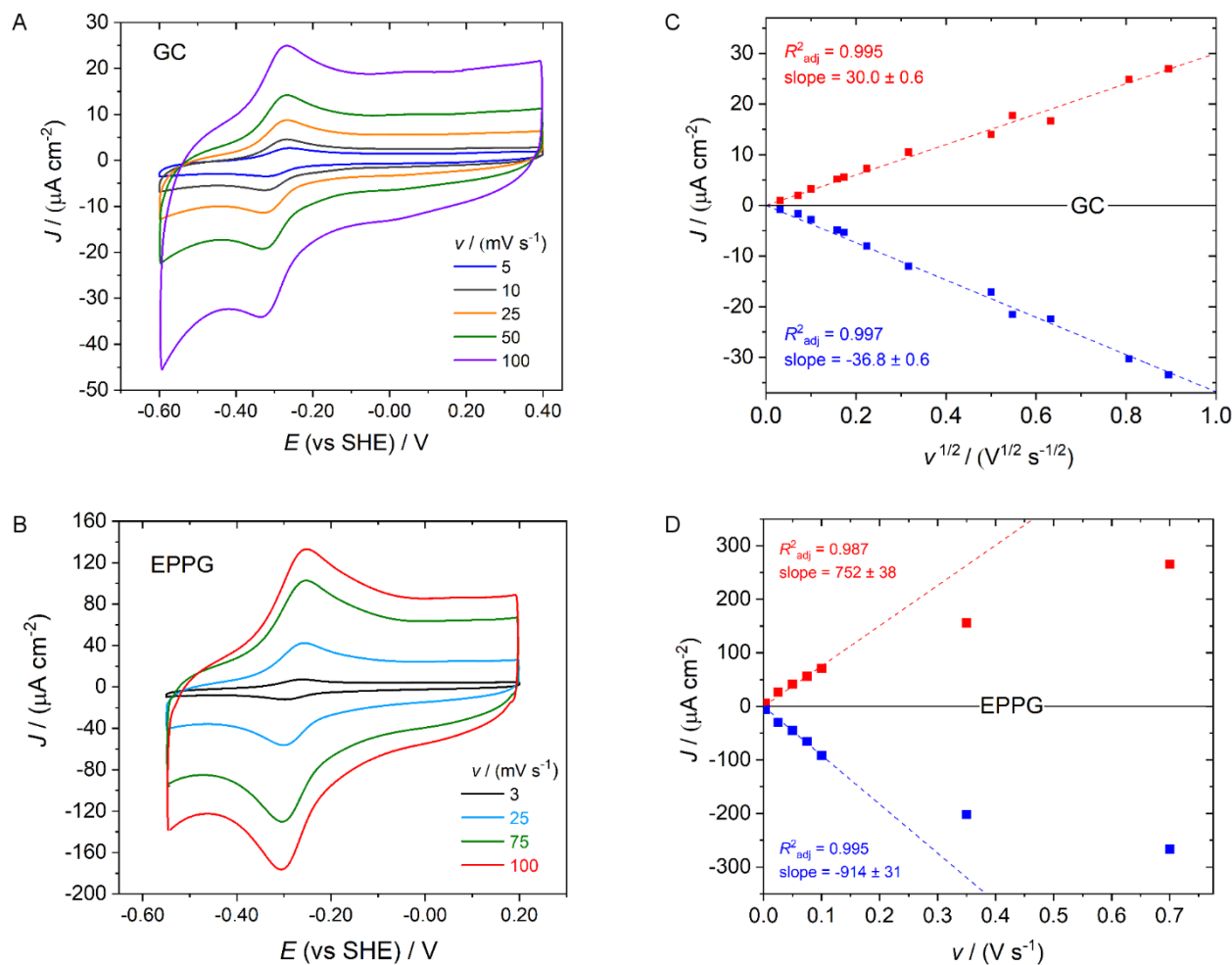


Figure 5. Cyclic voltammograms (a, b) and dependency of the cathodic and anodic currents on scan rate (c, d) for p(BMV-HET_{PFD}) hydrogel films on GC and EPPG electrodes. Background capacitive current was subtracted and the intercept of linear regression functions was forced through the origin; current densities at scanning rates of 0.35 V s⁻¹ and 0.70 V s⁻¹ were excluded from linear regression calculations in plot (d). (See Figure S13 for more voltammograms). Conditions: 2 μ L drop casting, supporting electrolyte TrisHCl 20 mM (GC) or 50 mM (EPPG) / NaCl 50 mM, pH 7.6.

This shift to higher redox potentials was anticipated, having been consistently observed for redox polymers in which a viologen derivative is anchored to a positively charged macromolecular matrix.^{[27a, 27d, 34, 37] [38]} It is due to the polyelectrolyte nature of the redox hydrogel, in which the electrostatic, excluded volume, and van der Waals interaction fields couple in a complex way and determine the free energy of the system.^[39] As a result, the formal potential of viologen moieties in p(BMV-HET_{PFD}) hydrogels is 50 mV more positive than that of [4Fe-4S] clusters of DbH-[NiFeSe] (Figure S13),^[22, 40] thus providing a sufficient driving force for ET between the hydrogenase and the redox matrix.

For modified GC electrodes, peak-to-peak separation (ΔE_p) at low scanning rates was \sim 50 mV, close to the 57 mV expected for a reversible monoelectronic diffusion-controlled redox system.^[41] At increasing scan rates, background-subtracted peak current densities J increased linearly with the square root of scan rate $v^{1/2}$ (Figure 5 c), indicating that electron transfer within the hydrogel film is governed by semi-infinite linear diffusion.^[42] According to the Randles-Sevcik equation, the slope of the linear dependency scales as:

$$\text{slope} \propto C \left(\frac{D_{CT}}{T} \right)^{1/2} \quad (1)$$

where C is concentration of redox species, D_{CT} is the apparent charge-transport diffusion coefficient, and T is temperature. The slope measured for the oxidation of Vio⁺⁺ moieties in p(BMV-HET_{PFD}) (3.0×10^{-5} A cm⁻² V^{-1/2}s^{1/2}) is 5.1 times higher than what observed for rubredoxin in RdHET-based AbRxHs on GC.^[14] Since equilibrium concentration of protein units is expected to be similar in the two hydrogels, D_{CT} must be at least one order of magnitude higher in the biohybrid matrix. This result was expected in virtue of the smaller size - hence higher D_{phys} - of methylviologen as compared to rubredoxin.^[43] Nonetheless, the implied D_{CT} is still 2 to 3 orders of magnitude lower than what reported for a methyl viologen-polyethylenimine hydrogel ($D_{CT} = 4.7 \times 10^{-9}$ cm² s⁻¹).^[29a] A possible explanation involve inter-wire charge transfer being hindered by limited surface contact and/or high distance; and the limited Brownian motion of large rigid nanofibers diminishing the collision frequency of redox sites.^[43-44] A different behaviour was observed for modified EPPG electrodes (Figure 5 b, d): compared to analogous GC electrodes, higher current densities were recorded at all scanning rates and the amount of faradaic charge exchanged during the reduction of Vio⁺⁺ moieties was 8 times higher ($v = 100$ mV s⁻¹).

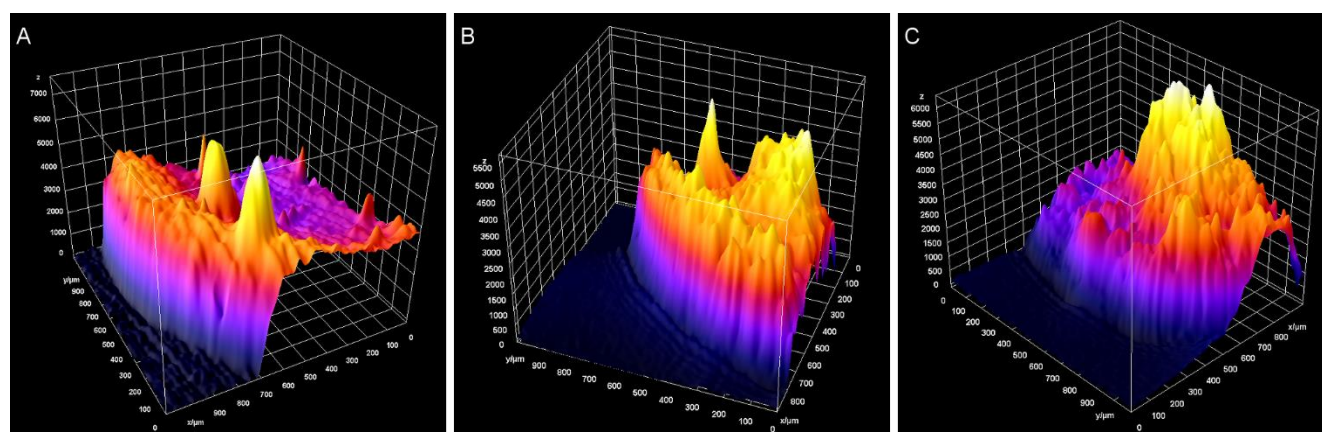


Figure 6. Topography of (A) single-layer electroactive p(BMV-HET_{PFD}), and (B) single-layer and (C) double layer p(BMV-HET_{PFD}) / DbH-[NiFeSe] bioelectrocatalytic hydrogel films drop-cast on a glass slide. The vertical scale is the same for all graphs, but it is in arbitrary units, whereas x- and y-axis are in μm .

Also, linear regression between peak current density J and $v^{1/2}$ is less convincing (Figure S14b): instead J scales tightly with v up to 100 mV s^{-1} as in a surface-confined electron transfer process (Figure 5 d), but the relationship breaks down at higher scanning rates. Lastly, ΔE_p is 27 mV at a low scanning rate — i.e. lower than the 57 mV expected for a reversible mono-electronic diffusion-controlled redox system — and increases almost linearly with $v^{1/2}$ to reach 51 mV at 100 mV s^{-1} and 89 mV at 700 mV s^{-1} (Figure S13d).

Detailed mechanistic investigation of these phenomena is beyond the scope of this study, but the role played by the EPPG surface as well as the nanostructured polyelectrolyte nature of the electroactive layer shall be taken into account. In particular, the chemical heterogeneity on the edge plane (with aromatic, hydrophilic, and carboxylate functionalities),^[45] the topological roughness of the EPPG surface and the presence of narrow basal plane terraces a few micrometres long^[46] make it particularly suitable for the adsorption of p(BMV-HET_{PFD}) nanowires. Furthermore, as reported for simpler redox polyelectrolyte films,^[47] the electrochemistry of AbRxHs is the result of a number of molecular processes (i.e. counter-ion diffusion, ion pairing, water transport, nanofibers rearrangement) that are linked to electron current density and are complex to model.^[48]

Concerning the stability of the electroactive layer on EPPG, after 3 days in the supporting electrolyte the intensity of the anodic wave due to the oxidation of Vio⁺ moieties decreased by 45%, suggesting desorption and/or disassembly of the redox hydrogel film (Figure S15).

Bioelectrodes for H₂ oxidation were fabricated by imbedding [NiFeSe]-hydrogenase from *Desulfomicrobium baculatum* (DbH-[NiFeSe]) into the AbRxH films coating carbon electrodes. Two different protocols were implemented, which involved the same amount of enzyme being applied onto the electrode.

In the first protocol, single-layer bioelectrocatalytic films were obtained by drop casting $3 \mu\text{L}$ of p(BMV-HET_{PFD}) fibrils suspension on the electrode followed by drying in the open atmosphere. The dry film was then swollen with $2 \mu\text{L}$ of buffered DbH-[NiFeSe] solution (pH 7.6), which also effected physical cross-linking by changing the surface charge of the nanofibrils. We postulated that, during the swelling process, part of the

negatively charged enzyme ($pI = 5.7$) would penetrate the nanofibers mesh and be entrapped by electrostatic interaction with the multiple positive charges on the nanofibers.^[49] Close inspection of the swelling process, however, revealed that most of the enzyme solution was not absorbed by the film at equilibrium, and was effectively wasted.

In an attempt to increase the efficiency of immobilization, a second protocol was tested in which the enzyme was pre-mixed with an equal volume of nanofibril suspension before being applied to electrode. Hence, double-layer electrocatalytic films were prepared by drop coating a first layer of p(BMV-HET_{PFD}) as describe above, followed by drop casting $2 \mu\text{L}$ or $4 \mu\text{L}$ of a 1:1 mixture of p(BMV-HET_{PFD}) / DbH-[NiFeSe] on the top of it, drying in the open atmosphere and immersion in the working electrolyte to complete electrostatic cross-linking.

Topography of the electroactive and bioelectrocatalytic hydrogel films obtained in this manner is shown in Figure 6. Compared to a single-layer p(BMV-HET_{PFD}) film (a), the addition of enzyme resulted in an accumulation of material at the centre of the film disk (b and c), as indicated by the increased thickness, while the footprint of the film remained unchanged. The effect was particularly pronounced for double-layer electrocatalytic films due to the further addition of p(BMV-HET_{PFD}) fibres.

Figure 7 depicts cyclic voltammograms obtained under Ar (solid line) and H₂ atmosphere (dashed line) for GC (a) and EPPG electrodes (b) modified with p(BMV-HET_{PFD}) / DbH-[NiFeSe] hydrogel coatings. Experiments were realized under quiescence conditions with a supporting electrolyte solution saturated either with Ar or with H₂; while gentle flushing of the cell head-space with the appropriate gas was maintained throughout the experiment. Under Ar atmosphere, the redox couple for the first viologen reduction was clearly observed for double-layer electrodes (Figure 7 a, b and Figure S16), but the anodic wave was systematically more intense than the cathodic one. This effect is probably due to slow hydrogen evolution taking place at low potentials, followed by rapid H₂ oxidation at higher ones, DbH-[NiFeSe] being a poor catalyst for HER but very active toward H₂ oxidation.^[22] In the case of single-layer GC electrodes, a small HER catalytic wave was indeed visible (Figure S16a).

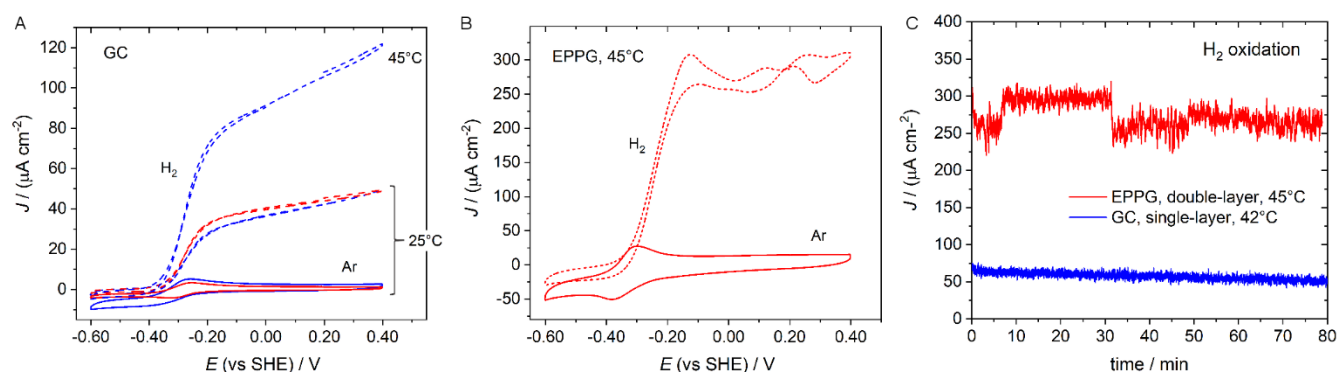


Figure 7. Cyclic voltammograms under quiescent conditions of modified GC (a) and EPPG (b) electrodes (scan rate 10 mV s^{-1}). Curves for single-layer (blue series) and double-layer (red series) p(BMV-HET_{PFD}) / DbH-[NiFeSe] hydrogel coatings under Ar (solid line) or H₂ atmosphere (dashed line) are shown. (c) Chronoamperometry at $E = +0.20 \text{ V}$ (GC) and $+0.00 \text{ V}$ (EPPG) under H₂ atmosphere. Coating volumes: GC single-layer, 3 μL fibrils + 2 μL enzyme; GC double-layer, 4 μL fibrils + 4 μL mix; EPPG double-layer, 3 μL fibrils + 2 μL mix. Supporting electrolyte TrisHCl 20 mM (50 mM for chronoamperometry GC) / NaCl 50 mM, pH 7.6.

Under H₂ atmosphere, pronounced catalytic waves were observed that are centred at the formal potential of the viologen electron relays. Since the latter is 150 to 170 mV more positive than the 2H⁺ / H₂ couple ($E^{\circ}_{\text{H}^+/\text{H}_2} = -0.449 \text{ V}$ at pH 7.6), the MET chain involving BMV moieties is limiting the turnover of the enzyme and DET can be excluded. According to the model of Léger,^[50] the active site of a multicenter redox enzyme feels the potential of a ET relay under the condition that the ET chain limits the enzymatic turnover. In this case, the ET relay acts as a Nernst buffer and protects the enzyme from high potential deactivation. However, if enzymatic turnover is limiting, fast ET chains involving artificial electron relays will display the same properties as the direct ET of enzymes directly adsorbed to electrodes, i.e. a catalytic wave centred on the redox potential of the enzyme's active site or of the substrate. In this case, protection from high potential would not be achieved.

Two control experiments were conducted with the enzyme either directly adsorbed on a EPPG electrode, or immobilized within an hydrogel of electroinactive p(HET_{PFD}) fibrils at the surface of the electrode. Similar results were obtained with the two coating protocols (Figure S12): under Ar atmosphere, the [4Fe-4S] electron-transfer signals of the enzyme are clearly visible after subtraction of the capacitive current ($E_{1/2} = -0.28$ and -0.35 V , respectively).^[22, 40] In the presence of H₂, an anodic wave starts at -0.40 V ($E^{\circ}_{\text{H}^+/\text{H}_2} = -0.449 \text{ V}$ at pH 7.6) but levels off between -0.20 V (co-immobilization) and 0.0 V (direct adsorption) due to oxidative inactivation of the enzyme.^[5] Reactivation takes place when the potential is scanned to negative values and a new, slightly less intense, anodic wave is observed in the following cycle.

For comparison, with p(BMV-HET_{PFD})-modified electrodes no oxidative inactivation of the enzyme took place at applied potentials as high as $+0.40 \text{ V}$. Also, when DbH-[NiFeSe] was immobilized within an hydrogel of electroinactive p(HET_{PFD}) fibrils, the catalytic current due to DET ($E = -0.20 \text{ V}$, $T = 25 \text{ }^{\circ}\text{C}$) was $0.21 \mu\text{A}$; whereas the same experiment carried out using p(BMV-HET_{PFD}) fibrils afforded a catalytic current of $1.3 \mu\text{A}$ (single-layer trace in Figure 7 a for a film area of 0.049 cm^2). Hence, the AbRxH effectively mediates electron transfer between the electrode and the hydrogenase and acts as a Nernst buffer protecting it from high potential deactivation.

Single- and double-layer coatings of GC electrodes lead to similar catalytic current profiles (Figure 7 a, series at 25°C), with a monotonic increase of current density with applied potential that slows down above -0.15 V but never reaches a plateau. This behaviour is independent of operating temperature and suggests that H₂ diffusion is not limiting catalytic current. In terms of electrocatalytic efficiency, then, the two coating protocols seem to be equivalent.

It is worth noting that current density due to H₂ oxidation at $+0.40 \text{ V}$ and $45 \text{ }^{\circ}\text{C}$ was 6 times higher than previously obtained at $60 \text{ }^{\circ}\text{C}$ with [NiFe] hydrogenase from *Aquifex aeolicus* embedded in RdHET-based AbRxH (a GC electrode was used in both cases),^[13] thus confirming the relevance of the new bioelectrode design. Under continuous turnover conditions at $+0.20 \text{ V}$, a slow but steady decline in catalytic current was observed, and after 80 min. only $\sim 65 \%$ of the initial activity remained (Figure 7 c). A complementary experiment (Figure S17) showed that the loss in catalytic current matches the reduction in charge exchanged during cyclic voltammetry for the reduction/oxidation of viologen moieties in the matrix. Excluding hydrolysis or degradation of BMV groups, it follows that gradual exfoliation and/or disassembly of the hydrogel is the main cause for the limited stability of the electrode over time. Enzyme inactivation and/or diffusion away from the electrode surface cannot be excluded though.

Results with modified EPPG electrodes were rather different (Figure 7 b). For applied potentials higher than -0.15 V , the monotonic increase of current density stopped and J started oscillating around a plateau of $\sim 270 \mu\text{A cm}^{-2}$. This value is over three-times higher than the current density recorded for modified GC electrodes at the same potential ($E = -0.15 \text{ V}$) and temperature ($45 \text{ }^{\circ}\text{C}$), the only other difference being the coating protocol – which was previously found to have little influence on catalytic currents (see Figure 7 a, series at 25°C).

Current density fluctuations of $\pm 7\%$ with a period of $\sim 1 \text{ min}$ were also recorded in chronoamperometric experiments under continuous H₂ oxidation conditions at $+0.00 \text{ V}$, but average current did not decline over an 80 min period, thus proving the robustness of the bioelectrode on this time scale (Figure 7 c). The fluctuations in J at high potential might be due to local fluctuations in substrate transport, pH and/or nanofibres morphology that do not take place at the slower reaction rates achieved with GC electrodes.

Conclusion

An artificial amyloid-based redox hydrogel was designed for mediating electron transfer from a [NiFeSe] hydrogenase to an electrode. Starting from a mutated prion-forming domain of fungal protein HET-s, a hybrid redox protein was synthesized that is capable of self-assembling into structurally homogenous nanofibrils in a predictable way. Molecular modelling confirmed that redox groups are loosely aligned along the fibril's axis and tethered to the central solenoid via a long flexible polypeptide chain. By exploring its conformational space in solution, the latter enables self-exchange reactions among the fibril-bound oxidized/reduced redox groups and, ultimately, mediates electron transport between the hydrogenase and the electrode.

At high concentration, a sudden change in surface charge of the fibrils leads to their lateral association into protein nanofibres and physical cross-linking through non-covalent interactions. This property was exploited to prepare redox hydrogel films that are capable of immobilizing a hydrogenase at the surface of carbon electrodes under mild conditions. Topography investigations revealed some accumulation of material both at the centre and at the outer rim of the circular deposit, but no "coffee-ring effect".

Based on these properties, new bioelectrodes for the electrocatalytic oxidation of H₂ were fabricated that afforded catalytic current densities of 270 $\mu\text{A cm}^{-2}$ under quiescent conditions for over one hour (applied overpotential 0.33 V). Gradual desorption and/or disassembly of the hydrogel appears to be the main factor limiting electrode stability over time, and further work is needed to improve film stability.

Although comparison between different systems is delicate (different hydrogenases, different amounts of enzyme, different temperatures, different pressures of H₂, etc.), the recorded catalytic current densities with double-layer EPPG electrodes (0.61 pmol of enzyme / cm²; quiescent conditions, no H₂ overpressure) are between 25% and 100 % of those reported by Plumeré et al. for DvMF [NiFe] hydrogenase / viologen-polyethylenimine catalytic hydrogel films (5.2 nmol of enzyme / cm²; GC rotating disc electrode, 1 bar of H₂).^[27d]

Conductive nanofibers featuring aryl-viologen groups were recently obtained by the self-assembly of a short peptide,^[51] but their ability to mediate electron transfer to an enzyme was not investigated. What is more, nanofibrils based on HET_{PFD} offer a wide scope for the rational design of monodimensional nanomaterials though site-directed mutagenesis and post-expression functionalization of the monomeric prion-forming domain, thanks to their intrinsic robustness, structural complexity and homogeneity.

Acknowledgements

This work has been partially supported by Labex ARCANÉ and CBH-EUR-GS (ANR-17-EURE-0003). We thank the NanoBio-ICMG Platform (FR 2607, Grenoble) for granting access to the Electron Microscopy and Mass Spectrometry facilities. This work used the platforms of the Grenoble Instruct-ERIC centre (ISBG; UMS 3518 CNRS-CEA-UGA-EMBL), part of the Grenoble Partnership for Structural Biology (PSB), supported by FRISBI (ANR-10-INBS-05-02) and GRAL, financed by the University Grenoble Alpes graduate school (*Ecoles Universitaires de Recherche*) CBH-EUR-GS (ANR-17-EURE-0003). Finally, we

thank Dr. J. Tan for the purification of Cys-HET_{PFD} samples, Dr. S. Ménage for useful discussions and suggestions, and Dr. J. Willison for proofreading the manuscript.

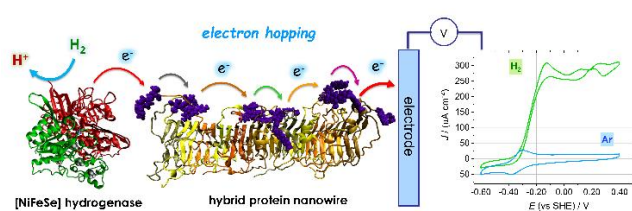
Keywords: hybrid prion forming domain • supramolecular polymer • protein nanowire • redox hydrogel • bioelectrocatalysis

- [1] a) J. Masa, W. Schuhmann, *Nano Energy* **2016**, *29*, 466-475; b) H. Chen, F. Dong, S. D. Minter, *Nature Catalysis* **2020**.
- [2] D. P. Hickey, R. D. Milton, M. Rasmussen, S. Abdellaoui, K. Nguyen, S. D. Minter, in *Electrochemistry: Volume 13, Vol. 13*, The Royal Society of Chemistry, **2016**, pp. 97-132.
- [3] a) F. A. Armstrong, H. A. O. Hill, N. J. Walton, *Accounts of Chemical Research* **1988**, *21*, 407-413; b) A. A. Karyakin, *Bioelectrochemistry* **2012**, *88*, 70-75.
- [4] K. A. Vincent, A. Parkin, F. A. Armstrong, *Chemical Reviews* **2007**, *107*, 4366-4413.
- [5] S. Gentil, S. M. Che Mansor, H. Jamet, S. Cosnier, C. Cavazza, A. Le Goff, *ACS Catalysis* **2018**, *8*, 3957-3964.
- [6] A. Heller, *Current Opinion in Chemical Biology* **2006**, *10*, 664-672.
- [7] A. Ruff, *Current Opinion in Electrochemistry* **2017**, *5*, 66-73.
- [8] a) A. Kumari, B. Ahmad, *RSC Advances* **2019**, *9*, 37424-37435; b) B. H. Pogostin, S. Linse, U. Olsson, *Langmuir* **2019**, *35*, 16536-16544.
- [9] a) M. Wehner, F. Würthner, *Nature Reviews Chemistry* **2020**, *4*, 38-53; b) S. Koutsopoulos, *Journal of Biomedical Materials Research Part A* **2016**, *104*, 1002-1016; c) G. Fichman, E. Gazit, *Acta Biomaterialia* **2014**, *10*, 1671-1682; d) J. D. Tang, C. Mura, K. J. Lampe, *J. Am. Chem. Soc.* **2019**, *141*, 4886-4899; e) L. Yang, H. Li, L. Yao, Y. Yu, G. Ma, *ACS Omega* **2019**, *4*, 8071-8080; f) S. Das, R. Kumar, N. N. Jha, S. K. Maji, *Advanced Healthcare Materials* **2017**, *6*, 1700368.
- [10] R. Wang, X. Yang, L. Cui, H. Yin, S. Xu, *Biomolecules* **2019**, *9*.
- [11] A. J. Baldwin, R. Bader, J. Christodoulou, C. E. MacPhee, C. M. Dobson, P. D. Barker, *J. Am. Chem. Soc.* **2006**, *128*, 2162-2163.
- [12] D. Leys, N. S. Scrutton, *Current Opinion in Structural Biology* **2004**, *14*, 642-647.
- [13] S. Rengaraj, R. Haddad, E. Lojou, N. Duraffourg, M. Holzinger, A. Le Goff, V. Forge, *Angew. Chem., Int. Ed.* **2017**, *56*, 7774-7778.
- [14] L. Altamura, C. Horvath, S. Rengaraj, A. Rongier, K. Elouarzaki, C. Gondran, A. L. B. Maçon, C. Vendrely, V. Bouchiat, M. Fontecave, D. Mariolle, P. Rannou, A. Le Goff, N. Duraffourg, M. Holzinger, V. Forge, *Nature Chemistry* **2017**, *9*, 157-163.
- [15] A. Balguerie, S. D. Reis, C. Ritter, S. Chaignepain, B. Couly - Salin, V. Forge, K. Bathany, I. Lascu, J. M. Schmitter, R. Riek, S. J. Saupé, *The EMBO Journal* **2003**, *22*, 2071-2081.
- [16] A. Balguerie, S. Dos Reis, B. Couly - Salin, S. Chaignepain, M. Sabourin, J. M. Schmitter, S. J. Saupé, *Journal of Cell Science* **2004**, *117*, 2599-2610.
- [17] P. Hosseinzadeh, Y. Lu, *Biochim Biophys Acta* **2016**, *1857*, 557-581.
- [18] a) C. Ritter, M.-L. Maddelein, A. B. Siemer, T. Luhrs, M. Ernst, B. H. Meier, S. J. Saupé, R. Riek, *Nature* **2005**, *435*, 844-848; b) C. Wasmer, A. Lange, H. Van Melckebeke, A. B. Siemer, R. Riek, B. H. Meier, *Science* **2008**, *319*, 1523-1526.
- [19] a) A. Daskalov, M. Gantner, M. A. Walti, T. Schmidlin, C. N. Chi, C. Wasmer, A. Schutz, J. Ceschin, C. Clave, S. Cescau, B. Meier, R. Riek, S. J. Saupé, *Plos Pathogens* **2014**, *10*; b) W. Wan, G. Stubbs, *PNAS* **2014**, *111*, 5201-5206.

- [20] R. Sabaté, U. Baxa, L. Benkemoun, N. Sánchez de Groot, B. Couлары-Salin, M.-I. Maddelein, L. Malato, S. Ventura, A. C. Steven, S. J. Saupé, *Journal of Molecular Biology* **2007**, *370*, 768-783.
- [21] W. Close, M. Neumann, A. Schmidt, M. Hora, K. Annamalai, M. Schmidt, B. Reif, V. Schmidt, N. Grigorieff, M. Fändrich, *Nature Communications* **2018**, *9*, 699.
- [22] A. Parkin, G. Goldet, C. Cavazza, J. C. Fontecilla-Camps, F. A. Armstrong, *Journal of the American Chemical Society* **2008**, *130*, 13410-13416.
- [23] A. Ruff, J. Szczeny, S. Zacarias, I. A. C. Pereira, N. Plumeré, W. Schuhmann, *ACS Energy Letters* **2017**, *2*, 964-968.
- [24] a) G. A. Grant, in *Current Protocols in Protein Science*, John Wiley & Sons, Inc., **2001**; b) C. D. Spicer, B. G. Davis, *Nature Communications* **2014**, *5*, 4740; c) O. Boutureira, G. J. L. Bernardes, *Chemical Reviews* **2015**, *115*, 2174-2195.
- [25] a) G. A. Rogers, N. Shaltiel, P. D. Boyer, *J. Biol. Chem.* **1976**, *251*, 5711-5717; b) E. Calce, M. Leone, L. Monfregola, S. D. Luca, *Organic Letters* **2013**, *15*, 5354-5357.
- [26] H. Tatsumi, K. Takagi, M. Fujita, K. Kano, T. Ikeda, *Analytical Chemistry* **1999**, *71*, 1753-1759.
- [27] a) L. H. Eng, M. Elmgren, P. Komlos, M. Nordling, S.-E. Lindquist, H. Y. Neujahr, *The Journal of Physical Chemistry* **1994**, *98*, 7068-7072; b) A. L. De Lacey, M. Detcheverry, J. Moiroux, C. Bourdillon, *Biotechnology and Bioengineering* **2000**, *68*, 1-10; c) A. A. Karyakin, D. V. Vinogradova, S. V. Morozov, E. E. Karyakina, *Electrochimica Acta* **2010**, *55*, 7696-7700; d) N. Plumeré, O. Rüdiger, A. A. Oughli, R. Williams, J. Vivekananthan, S. Pöller, W. Schuhmann, W. Lubitz, *Nature Chemistry* **2014**, *6*, 822.
- [28] a) J. A. Farrington, M. Ebert, E. J. Land, K. Fletcher, *Biochimica Et Biophysica Acta* **1973**, *314*, 372-381; b) R. N. Thorneley, *Biochimica Et Biophysica Acta* **1974**, *333*, 487-496; c) Q. Lin, Q. Li, C. Batchelor-McAuley, R. G. Compton, *Physical Chemistry Chemical Physics* **2013**, *15*, 7760-7767.
- [29] a) V. Fourmond, S. Stapf, H. Li, D. Buesen, J. Birrell, O. Rüdiger, W. Lubitz, W. Schuhmann, N. Plumeré, C. Léger, *Journal of the American Chemical Society* **2015**, *137*, 5494-5505; b) A. A. Oughli, F. Conzuelo, M. Winkler, T. Happe, W. Lubitz, W. Schuhmann, O. Rüdiger, N. Plumeré, *Angewandte Chemie International Edition* **2015**, *54*, 12329-12333; c) A. A. Oughli, A. Ruff, N. P. Boralugodage, P. Rodríguez-Maciá, N. Plumeré, W. Lubitz, W. J. Shaw, W. Schuhmann, O. Rüdiger, *Nature Communications* **2018**, *9*, 864; d) J. Szczeny, N. Marković, F. Conzuelo, S. Zacarias, I. A. C. Pereira, W. Lubitz, N. Plumeré, W. Schuhmann, A. Ruff, *Nature Communications* **2018**, *9*, 4715; e) H. Li, D. Buesen, S. Dementin, C. Léger, V. Fourmond, N. Plumeré, *Journal of the American Chemical Society* **2019**, *141*, 16734-16742.
- [30] a) E. M. Kosower, J. L. Cotter, *Journal of the American Chemical Society* **1964**, *86*, 5524-5527; b) T. Watanabe, K. Honda, *The Journal of Physical Chemistry* **1982**, *86*, 2617-2619; c) J. F. Stargardt, F. M. Hawkrigde, *Analytica Chimica Acta* **1983**, *146*, 1-8.
- [31] S. M. Kelly, T. J. Jess, N. C. Price, *Biochimica et Biophysica Acta (BBA) - Proteins and Proteomics* **2005**, *1751*, 119-139.
- [32] N. Mizuno, U. Baxa, A. C. Steven, D. Caspar, *PNAS* **2011**, *108*, 3252.
- [33] a) D. Willmer, K. A. Baldwin, C. Kwartnik, D. J. Fairhurst, *Physical Chemistry Chemical Physics* **2010**, *12*, 3998-4004; b) H. Hu, R. G. Larson, *The Journal of Physical Chemistry B* **2006**, *110*, 7090-7094; c) M. Anyfantakis, D. Baigl, *ChemPhysChem* **2015**, *16*, 2726-2734; d) R. D. Deegan, O. Bakajin, T. F. Dupont, G. Huber, S. R. Nagel, T. A. Witten, *Nature* **1997**, *389*, 827-829; e) R. D. Deegan, O. Bakajin, T. F. Dupont, G. Huber, S. R. Nagel, T. A. Witten, *Physical Review E* **2000**, *62*, 756-765.
- [34] H. Li, D. Buesen, R. Williams, J. Henig, S. Stapf, K. Mukherjee, E. Freier, W. Lubitz, M. Winkler, T. Happe, N. Plumeré, *Chemical Science* **2018**, *9*, 7596-7605.
- [35] a) P. Marquet, B. Rappaz, P. J. Magistretti, E. Cuche, Y. Emery, T. Colomb, C. Depeursinge, *Opt. Lett.* **2005**, *30*, 468-470; b) B. Rappaz, P. Marquet, E. Cuche, Y. Emery, C. Depeursinge, P. J. Magistretti, *Opt. Express* **2005**, *13*, 9361-9373.
- [36] C. L. Bird, A. T. Kuhn, *Chemical Society Reviews* **1981**, *10*, 49-82.
- [37] a) T. Nakahira, M. Graetzel, *J. Phys. Chem.* **1984**, *88*, 4006-4010; b) T. Janoschka, N. Martin, U. Martin, C. Friebe, S. Morgenstern, H. Hiller, M. D. Hager, U. S. Schubert, *Nature* **2015**, *527*, 78-81.
- [38] To the best of our knowledge, the sole exception is a paper by Willner et al. (The Journal of Physical Chemistry **1993**, *97*, 7264-7271), in which a 0.25V shift toward more negative potentials is reported for a viologen-polyethylenimine system at pH 7. The shift decreases monotonically with decreasing pH and vanishes at pH = 1. The authors speculate that in neutral and basic solutions, electron-donating amino groups of the polymer backbone can form donor-acceptor charge-transfer complexes with the bipyridinium units, thereby transforming the redox groups into relatively electron-rich entities that require more negative potentials for their reduction. By contrast, in their recent and extensive work on branched and dendritic viologen-polyethylenimine hydrogels, a -0.15 V shift toward more potentials was systematically observed by Lubitz, Schuhmann and Plumeré.
- [39] M. Tagliazucchi, E. J. Calvo, in *Chemically Modified Electrodes* (Eds.: R. C. Alkire, D. M. Kolb, J. Lipkowski, P. N. Ross), John Wiley & Sons, Inc., **2009**, pp. 57-115.
- [40] M. Teixeira, I. Moura, G. Fauque, D. V. Dervartanian, J. Legall, H. D. Peck Jr, J. J. G. Moura, B. H. Huynh, *European Journal of Biochemistry* **1990**, *189*, 381-386.
- [41] J. M. Savéant, C. Costentin, *Elements of Molecular and Biomolecular Electrochemistry: An Electrochemical Approach to Electron Transfer Chemistry*, John Wiley and Sons, Hoboken, NJ, USA, **2019**.
- [42] A. J. Bard, L. R. Faulkner, *Electrochemical Methods: Fundamentals and Applications, 2nd Edition*, John Wiley & Sons, **2001**.
- [43] K. Sato, R. Ichinoi, R. Mizukami, T. Serikawa, Y. Sasaki, J. Lutkenhaus, H. Nishide, K. Oyaizu, *Journal of the American Chemical Society* **2018**, *140*, 1049-1056.
- [44] L. Bello, C. E. Sing, *Macromolecules* **2020**, *53*, 7658-7671.
- [45] R. L. McCreery, *Chemical Reviews* **2008**, *108*, 2646-2687.
- [46] A. N. Patel, S.-y. Tan, T. S. Miller, J. V. Macpherson, P. R. Unwin, *Analytical Chemistry* **2013**, *85*, 11755-11764.
- [47] a) Lyons, *Transport and Kinetics in Electroactive Polymers*, **1996**; b) G. Inzelt, in *Encyclopedia of Electrochemistry*, Wiley - VCH, **2007**, pp. 651-683.
- [48] M. Tagliazucchi, E. J. Calvo, I. Szeleifer, *Electrochimica Acta* **2008**, *53*, 6740-6752.
- [49] Note that the BMV moiety contributes two permanent positive charges to each BMV-HET protein.
- [50] C. Léger, F. Lederer, B. Guigliarelli, P. Bertrand, *Journal of the American Chemical Society* **2006**, *128*, 180-187.
- [51] D. E. Clarke, M. Olesińska, T. Mönch, B. Schoenaers, A. Stesmans, O. A. Scherman, *Chemical Communications* **2019**, *55*, 7354-7357.

RESEARCH ARTICLE

Entry for the Table of Contents



A biohybrid prion-forming domain was synthesized that is capable to undergo hierarchical self-assembly into single-stranded protein nanowires, nanofibres and supramolecular redox hydrogels. This property enabled us to immobilize a [NiFeSe] hydrogenase within a water-swollen network of conductive nanofibres via a gentle non-covalent cross linking process, while ensuring its wiring to carbon electrodes for electrocatalysis.